Defining Local Chemical Conditions in Magnetosomes of Magnetotactic Bacteria

Matthieu Amor, Damien Faivre, Jérôme Corvisier, Mickaël Tharaud, Vincent Busigny, Arash Komeili, Francois Guyot

Defining Local Chemical Conditions in Magnetosomes of Magnetotactic Bacteria

Matthieu Amor[1,2*], Damien Faivre[1], Jérôme Corvisier[3], Mickaël Tharaud[4], Vincent Busigny[4,5], Arash Komeili[2,6], François Guyot[7*]

[1]Aix-Marseille Université, CEA, CNRS, BIAM, 13108 Saint-Paul-lez-Durance, France

[2] Department of Plant and Microbial Biology, University of California, Berkeley, CA 94720-3102

[3] Mines ParisTech, PSL ResearchUniversity, Centre de Géosciences, 35 rue Saint Honoré, 77305 Fontainebleau Cedex, France

[4] Université de Paris, Institut de Physique du Globe de Paris, CNRS, Paris, F-75005, France

[5] Institut Universitaire de France, Paris 75005, France

[6] Department of Molecular and Cell Biology, University of California, Berkeley, CA 94720-3200

[7] Institut de Minéralogie, de Physique des Matériaux et de Cosmochimie, Muséum National d'Histoire Naturelle, Sorbonne Université, UMR 7590 CNRS, 61 rue Buffon 75005 Paris, France

*Corresponding authors:
matthieu.amor@cea.fr (MA); francois.guyot@mnhn.fr (FG)

Keywords: Magnetite, Magnetosome, Bacterial Organelle, Biomineralization, Magnetotactic Bacteria

Abstract

Defining chemical properties of intracellular organelles is necessary to determine their function(s) as well as understand and mimic the reactions they host. However, the small size of bacterial and archaeal microorganisms often prevents to define local intracellular chemical conditions in a similar way to what has been established for eukaryotic organelles. This work proposes to use magnetite (Fe_3O_4) nanocrystals contained in magnetosome organelles of magnetotactic bacteria as reporters of elemental composition, pH and redox potential of an hypothetical environment at the site of formation of intracellular magnetite. This methodology requires combining recent single-cell mass spectrometry measurements together with elemental composition of magnetite in trace and minor elements. It enables a quantitative characterization of chemical disequilibria of 30 chemical elements between the intracellular and external media of magnetotactic bacteria, revealing strong transfers of elements with active influx or efflux processes that translate into elemental accumulation (Mo, Se, Sn) or depletion (Sr, Bi) in the bacterial internal medium of up to seven orders of magnitude relative to the extracellular medium. Using this concept, we show that chemical conditions in magnetosomes are compatible with a pH of 7.5 – 9.5 and a redox potential of -0.25 – -0.6 V.

Table of content

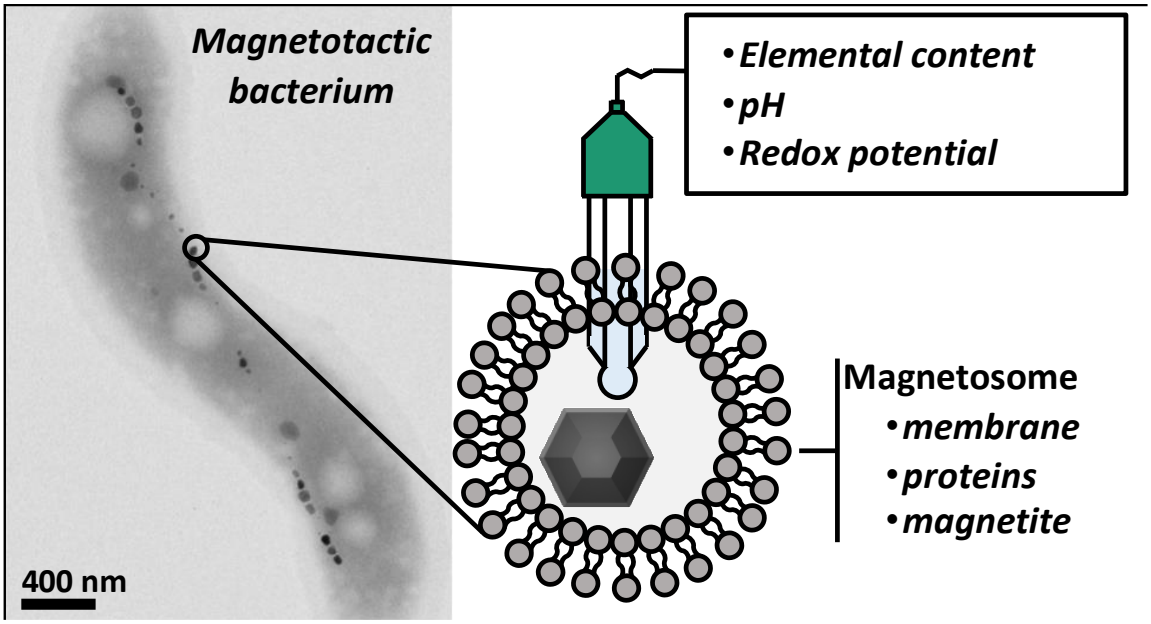

Introduction

Organelles are subcellular membrane-bounded structures executing key biochemical reactions. Even though they were originally considered as a hallmark of eukaryotic cells, many organelles have been discovered in bacteria and archaea including anamoxosomes [1], acidocalcisomes [2], or ferrosomes [3]. These compartments are physically separated from the cytoplasm. They generate a local well-defined environment with specific chemical properties that constrain the biochemical reactions occurring within this dedicated intracellular space. Determining these chemical specificities is critical to understand the biological reactions they host, their function(s), as well as for designing new technologies through synthetic biology approaches [4]. Successful investigations have characterized the pH and redox potential (Eh) homeostasis in eukaryotic organelles[5], mainly through methodologies involving fluorescent dyes or probes and subsequent sample imaging[5–10]. Similarly, fluorescent methodologies have been used to quantify and map incorporation of calcium and magnesium in intracellular structures for precipitation of biominerals [10–12]. However, the spatial resolution of these techniques prevents their use for small bacterial and archaeal organelles that can be as small as 50 nm in diameter or less. Alternative approaches must therefore be defined to constrain local chemical conditions in prokaryotic microorganisms.

Magnetosomes in magnetotactic bacteria (MTB) are bacterial organelles consisting of bi-layered lipid membranes containing a single crystal of magnetite [$Fe(II)Fe(III)_2O_4$] or greigite [$Fe(II)Fe(III)_2S_4$] (Fig. 1) [13]. They are aligned in chains, usually along the cell's long axis, and provide the bacteria with a permanent magnetic moment that is proposed to allow passive orientation along the geomagnetic field, facilitating the reach of optimum environmental conditions [14]. As evidenced in a few species that represent a small fraction of the whole MTB

diversity, magnetosome formation is genetically controlled, and requires ~30 genes mostly clustered in a specific portion of the genome [15]. Magnetosome vesicles first invaginate from the inner membrane [16]. A large amount of iron is then incorporated into the cytoplasm and/or periplasm of MTB [17] where it is stored as ferrihydrite-like species, and then partially reduced into soluble Fe(II) for delivery to magnetosomes and subsequent re-oxidation and precipitation into magnetite or greigite [18,19]. Accordingly, the composition and physico-chemical properties of the magnetosome internal medium are likely to vary over the biomineralization process. In magnetite-forming bacteria, the growth of newly formed magnetosomes is blocked until magnetite nucleation triggers further expansion and maturation of the magnetosome [20]. The signal generating such vesicle remodeling is unknown, and could correspond to specific protein content as recently proposed by Wan and co-workers who showed that growth of magnetosome vesicle is associated with processing of the protein MamD by MamE proteases[21]. In addition, vesicle remodeling could also be triggered by specific chemical properties of the magnetosome internal medium (e.g., elemental composition, pH, Eh). A detailed characterization of the chemical medium at the interface with magnetite would thus bring important insights into the biogenesis of magnetosomes.

In a previous study, the chemical composition in minor and trace elements of magnetite synthesized by the magnetotactic strain *Magnetospirillum magneticum* AMB-1 was determined (Fig. 1) [22]. Moreover, the partitioning of trace and minor elements between magnetite and the external solution was determined in the case of magnetite nanoparticles synthesized abiotically from Fe^{2+} and Fe^{3+} co-precipitation. In the present study, using the methodology for single-cell measurements of iron in AMB-1 developed recently [17], we are now able to estimate the concentration of dissolved iron in the aqueous solution in contact

with magnetite. When combined with the previous set of trace and minor elements in abiotic magnetite, single-cell iron measurements are used to determine the concentrations of chemical elements in a conceptual equivalent solution at thermodynamic equilibrium with magnetite. The pH and Eh values in this equivalent solution are also determined following this approach, and are contained in a domain around pH = 7.5 – 9.5 and Eh = -0.25 – -0.6 V, respectively. Such pH conditions are higher from the cytoplasmic and periplasmic values previously reported, which points to the specific local chemical conditions allowing magnetite formation.

Methods

Bacterial cultures

Magnetospirillum magneticum strain AMB-1 (ATCC700264) was cultivated for two days in 10-mL tubes following ATCC recommendations at 30°C under controlled atmosphere (90 % N_2, 10 % O_2). The sole iron source in bacterial growth media corresponded to Fe(III)-citrate added to the growth medium at 10, 50, 100, 200, 300 or 500 μM. Volume of cultures were kept constant in all conditions by adding an iron-free citrate solution. The pH of both Fe(III)-citrate and citrate solutions were first set at 6.9 (*i.e.* identical to growth medium) before addition to AMB-1 media. AMB-1 cells were recovered by centrifugation (8 000 g, 10 min) and washed three times in Phosphate Buffer Saline (PBS) to prevent cell lysis and remove iron from the growth media or adsorbed on the cell surfaces.

Single-cell mass spectrometry

The iron content in single AMB-1 cells was measured following a time-resolved mass spectrometry methodology that was previously developed [17]. Briefly, the concentration of iron

in PBS solutions containing bacteria was measured to ensure that no intracellular iron was lost during sample preparation. Bacteria were then diluted and nebulized into the plasma. Each cell forms an ion cloud containing the intracellular iron that is collected by the detector. At millisecond dwell times, the ion cloud produces a signal pulse, whose intensity is directly related to the number of ions in the cloud and therefore to the cell mass. Also, assuming constant nebulization efficiency, the number of detected pulses is directly related to the number of cells in the sample. Analyses were performed on an HR-ICP-MS Element II (ThermoScientific, Germany) located in an ISO 4 cleanroom at the *Institut de Physique du Globe de Paris* (France). ^{56}Fe was monitored in medium resolution (MR; R > 4000) as the separation power of the Element II in MR is high enough to resolve the main interference (*c.* $^{40}Ar^{16}O$ at m/z = 56). Externalized iron concentrations were determined averaging 9 data acquired with a 50 ms dwell time using the uFREASI software [23] for the intensity-concentration conversion.

Electron microscopy

Abiotic magnetite nanoparticles and cells were deposited on copper grids coated with a Formvar film, and observed with a Jeol J-2100 transmission electron microscope operating at 200 kV.

Thermodynamic calculations

Magnetite solubility simulations were performed using the geochemical code CHESS (CHemical Equilibrium of Species and Surfaces) [24] combined with the THERMODDEM database [25]. The starting solution contained magnetite at 5×10^{-3} M, which corresponds to the

concentration of magnetite in MTB cells (Tables S1 and 1). For solutions containing Fe^{2+} ligands, two compounds (L^{2-}) with logβ values of 5 and 10 were added to the starting solutions. The ligand was added in excess compared to Fe^{2+}, with a magnetite/ligand ratio of 3 (corresponding to the magnetite/ferritin ratio in MTB) (Table 1). The final concentrations of magnetite, total iron, Fe^{2+}, Fe(II)L and Fe^{3+} were calculated at 298 K for pH and Eh values ranging between 2 and 12, and -0.9 and 0.4 V, respectively. Because only magnetite is observed in MTB, distinct iron phases (goethite, hematite, lepidocrocite, maghemite, wustite and elemental iron) were excluded from the simulations. Finally, Fe^{2+} phase diagram under the same pH and Eh conditions was also simulated with the CHESS code.

Results and Discussion

Partition coefficients between abiotic magnetite nanoparticles and coexisting solutions

Incorporation of chemical elements other than iron into magnetite synthesized by co-precipitation of dissolved Fe^{2+} and Fe^{3+} in aqueous solution was recently measured [22]. The exchange reaction between iron and a chemical element X in magnetite and solution can be written as:

$$X_{solution} + Fe_{magnetite} \rightleftharpoons X_{magnetite} + Fe_{solution} \quad [1]$$

The partition coefficient ($K^{X/Fe}$) of an element X normalized to iron and describing the thermodynamics of partitioning between magnetite and the external solution in Eq. 1 is given by:

$$K^{X/Fe} = \frac{\{X_{magnetite}\}\{Fe_{solution}\}}{\{X_{solution}\}\{Fe_{magnetite}\}} \quad [2]$$

where $\{Fe_{solution}\}$ and $\{Fe_{magnetite}\}$ are the activities of iron in solution and magnetite, respectively, and $\{X_{solution}\}$ and $\{X_{magnetite}\}$ are the activities of an element X in solution and magnetite, respectively. In the case of an ideal aqueous solution, a standard system can be chosen in which the activities $\{Fe_{solution}\}$ and $\{X_{solution}\}$ are equal to the mass concentrations of Fe ($[Fe_{solution}]$) and X ($[X_{solution}]$) in solution expressed in ppb (i.e., part per billion corresponding to the mass of Fe or X in µg measured in 1 kg of solution). In a similar way, in the case of ideal mixing of the X in magnetite, a standard system can be chosen in which the activities $\{X_{magnetite}\}$ correspond to the mass concentrations in magnetite ($[X]_{magnetite}$) (i.e., the mass of element X in relation to the total mass of magnetite). In the case of iron, using a solvent-type reference system implies that:

$$\{Fe_{magnetite}\} = 1 \quad [3]$$

However, for most elements X, both in solution and in magnetite, mixing is not ideal which leads to:

$$\{X_{solution}\} = \gamma^{X}_{solution} \times [X_{solution}] \quad [4.1]$$

$$\{Fe_{solution}\} = \gamma^{Fe}_{solution} \times [Fe_{solution}] \quad [4.2]$$

where $\gamma^{X}_{solution}$ and $\gamma^{Fe}_{solution}$ are the activity coefficients of an element X and Fe in solution,

respectively, and:

$$\{X_{magnetite}\} = \gamma^{X}_{magnetite} \times [X_{magnetite}] \quad [5]$$

where $\gamma^{X}_{magnetite}$ is the activity coefficent of element X in magnetite. Using Eqs. 2, 4.1, 4.2 and 5, we write:

$$K^{X/Fe} = \frac{\gamma^{X}_{magnetite}\,\gamma^{Fe}_{solution}}{\gamma^{X}_{solution}} \times \frac{[X_{magnetite}]\,[Fe_{solution}]}{[X_{solution}]} \quad [6]$$

Finally, considering:

$$\Gamma = \frac{\gamma^{X}_{magnetite}\,\gamma^{Fe}_{solution}}{\gamma^{X}_{solution}} \quad [7]$$

and:

$$\mathrm{K}^{X/Fe}_{apparent} = \frac{[X_{magnetite}]\,[Fe_{solution}]}{[X_{solution}]} \quad [8]$$

we obtain:

$$\mathrm{K}^{X/Fe}_{apparent} = \frac{\mathrm{K}^{X/Fe}}{\Gamma} \quad [9]$$

The $K_{apparent}^{X/Fe}$ values can be obtained from the measurements of mass concentrations of each chemical element in magnetite and solution. Results are given in Table S1.

Chemical composition of biological magnetite nanoparticles and inference of elemental composition of coexisting solutions

Using the values of $K_{apparent}^{X/Fe}$ measured in the experiments of abiotic synthesis of magnetite (previous section and Table S1), we can now estimate the chemical composition of the equivalent solution which is the hypothetic aqueous fluid in thermodynamic equilibrium with magnetite within MTB cells. Activity coefficients in solution may vary between the conditions of abiotic magnetite precipitation and that of the equivalent solution, due mostly to differences in ionic strength. Using standard activity-concentration relations (e.g., extended Debye-Hückel), we observe that in most cases changes in ratios $\frac{\gamma_{solution}^{Fe}}{\gamma_{solution}^{X}}$ (Eq. 7) between the two conditions result in corrections on $K_{apparent}^{X/Fe}$ (Eq. 9) smaller than error bars (Table S1). We note that $\frac{\gamma_{solution}^{Fe}}{\gamma_{solution}^{X}}$ (Eq. 7) ratios may show larger differences between the two conditions of magnetite formation for highly charged cations (Al^{3+}), up to a factor of 25 which would still not have a significant effect on the comparison between abiotic and biological partition coefficients (Table S1). Moreover, the activity coefficient of element X in magnetite is likely very close between abiotic and biological magnetite given the similar crystal-chemical speciation of X[26–29]. Therefore, the assumption that the Γ parameters are close between those two conditions is reasonable in first approximation. We also note that the details of activity coefficients in the intracellular medium depend in a large part on specific interactions between the different metallic

elements and the proteome of MTB, and thus remain essentially unknown so far requesting a lot of data acquisition in the future. Under this assumption, and under the hypothesis of a thermodynamic equilibrium in element partitioning in the abiotic magnetite formation experiments, the concentrations of chemical elements in the equivalent solution ($[X]_{solution}$) can be determined using Eq. 8. In Eq. 8, the measured mass concentration of an element X in the biological magnetite, the mass concentration of iron in the equivalent solution from which biological magnetite precipitates, and the partition coefficients ($K_{apparent}^{X/Fe}$) are experimental data measured in abiotic magnetite precipitation experiments. The concentrations of trace and minor elements in AMB-1 magnetite ($[X]_{magnetite}$) are obtained from high-resolution – inductively coupled plasma – mass spectrometry data when bacteria were cultivated either in a 2-liter bioreactor (one replicate) or bottles (two replicates), which allowed us to assess the biological variability induced by varying external conditions (Table S2) [22]. Using the assumptions described above, it is then possible to infer a chemical composition of this equivalent aqueous solution in both bottle and bioreactor conditions if the concentration in dissolved iron (i.e., $[Fe_{solution}]$) can be estimated in the equivalent aqueous solution. A last assumption will be made here, according to which the intracellular concentration of iron is a first low-boundary approximation of the concentration in the equivalent solution. Then, a measurement of the intracellular concentration of iron, if technically possible, would provide the concentration of iron in the equivalent solution and thus of all elemental concentrations (Eq. 2). The first step to estimate the intracellular iron concentration is to measure the bulk iron content in MTB cells. The intracellular mass of iron contained in MTB at the population level has been estimated and typically ranged between 1.5 and 13 mg per g (dry weight) [30–32]. However, it has so far not been connected

to the number of cells in the population, preventing assessment of the bacterial iron content. Using a dry mass of single magnetotactic cell of 10^3 fg [33], we estimate a total mass of iron ranging between ~1 and 10 fg per cell. Recently, a mass spectrometry methodology has been developed for direct determination of the total mass of iron contained in AMB-1 bacteria at the single-cell level [17]. In the present study, we followed this method to measure the mass of iron in AMB-1 cells cultivated with iron added at various concentrations in the growth medium: 10, 50, 100, 200, 300 and 500 μM. Results showed a total mass of iron ranging between ~0.7 and 2.4 fg per cell (Fig. 2 and Table S3). They are in good agreement with previous measurements [17], and are compatible with the masses estimated from data obtained at the population level mentioned above [30–32]. Assimilating AMB-1 cells to a 3-μm long cylinder with a radius of 0.5 μm (Fig. 1), these masses transform into bulk iron intracellular concentrations ranging between $5.41 \pm 2.54 \times 10^{-3}$ M and $1.82 \pm 0.86 \times 10^{-2}$ M (Fig. 2 and Table S3).

The second step for estimating the dissolved iron concentration in the equivalent solution is to estimate the fraction of total cellular iron previously measured that is not dissolved but instead precipitated as magnetite or associated with iron-storage proteins (i.e., ferritins). Several research groups have characterized iron speciation in three strains of magnetospirilla: *Magnetospirillum magneticum* AMB-1, *Magnetospirillum gryphiswaldense* MSR-1 and *Magnetospirillum magnetotacticum* MS-1. Their findings are summarized in Table 1, and show that magnetite is far from being the sole iron reservoir in MTB. Ferritin-like structures and ferrous metabolites likely corresponding to ferrous sugar phosphates or to Fe^{2+} more or less complexed in the cytoplasm were also identified [34–37]. In AMB-1, magnetite represents 30 to 50 % of the total intracellular iron [37]. Such

fraction was found higher in MSR-1 (50-70 %) and MS-1 (80%). We note that additional works also determined the temporal evolution of iron speciation in AMB-1 and MSR-1 using X-ray absorption spectroscopy [38,39]. In these cases, bacteria were first cultivated under iron-starving conditions, which were shown to alter iron homeostasis and favor iron precipitation into magnetite [37]. We have not taken into account those X-ray absorption results for the present inference of dissolved intracellular iron concentrations because they were acquired in experimental conditions quite different from those of the present study. The concentration of dissolved iron in MTB was obtained from the difference between total iron concentration in cell and that of the other iron phases (magnetite, ferritins, etc.), and was determined from data in Tables S3 and 1. It ranges between $3.25 \pm 1.53 \times 10^{-4}$ and $1.09 \pm 0.51 \times 10^{-3}$ M (i.e., $1.81 \pm 0.85 \times 10^{4}$ and $6.09 \pm 2.85 \times 10^{4}$ ppb, respectively). Here, we consider that all dissolved iron corresponds to Fe(II) phases as shown by previous work [34,35] and present thermodynamic modeling (see below). These concentrations are close to (500 μM condition) or higher than (low initial iron conditions) the iron concentrations measured in the external growth medium (Tables 2 and S2), which suggests active uptake under iron-limited conditions and passive diffusion of Fe(II) between the intracellular medium and the external solution under iron-sufficient conditions, in good agreement with previous findings [18,40].

Using the results reported in Tables S1 and 1, the concentration of each tested element in the equivalent solution was then determined using Eq. 2 (Table 2). Results show a large variation, with concentrations ranging between 2.01 ± 0.10 ppb for strontium and $1.24 \pm 0.61 \times 10^{8}$ ppb for tin. These concentrations were then compared with the elemental concentrations in the residual bacterial medium after bacterial growth and magnetite

formation (Table 2). They showed much less variations, with most values ranging between 10^2 and 10^4 ppb.

Comparison of elemental concentrations in the equivalent solution and the external growth medium can provide further insight on the element transfer to AMB-1 magnetite. In the case of abiotic precipitation, the solution in contact with magnetite is directly accessible and the similarity between actual and calculated pH and Eh values (see below) is in favor of thermodynamic equilibrium between magnetite and solution. In this case, the supernatant of magnetite corresponds to the equivalent solution in equilibrium with magnetite. There is no obvious reason for which the biological equivalent solution should be close to the residual aqueous phase in the external culture medium. Indeed, bacterial cells possess efflux transporters of specific transition metals, heavy metals and metalloids to prevent toxicity [41]. The bacterial membranes may also create a physical barrier restricting the chemical elements in the growth medium to reach the location of magnetite formation. Alternatively, metals can be actively incorporated into the intracellular environment to maintain homeostasis (e.g., iron incorporation by MTB for magnetosome formation). A possibility we previously mentioned is that the composition of the equivalent solution could be close to that of the intracellular medium. In this case, the concentration ratios between the external residual medium and the equivalent solution (Table 2) give interesting indications on the efflux or active pumping of chemical elements between the external and the intracellular media. Three types of behavior are observed: (i) the ratio is much higher than 1 (> 10; i.e., efflux processes), which suggests that the element is evacuated from the intracellular medium where we assume magnetite is formed. This is observed for Ba, Bi, Co, Cu, In, La, Mg, Mn, Pb, Sr, Th, Tl, Y. Specifically, Sr and Bi showed strong depletion,

with a ratio of ~5×10^2 and 10^3, respectively. Such depletion may illustrate homeostasis of these elements, as Sr is known to act as a Ca antagonist and disturb Ca regulation that is essential for cell signaling [42]. (ii) The ratio is much lower than 1 (< 0.1; i.e., active pumping), which suggests that the element is actively incorporated and concentrated in the intracellular medium at the assumed location of magnetite formation in comparison with the external solution. This is the case for As, Ca, Cs, Ga, Mo, Rb, Se, Sn, Zn. Importantly, our methodology revealed extreme ratios for Mo (< 10^{-5}), Se (< 10^{-4}) and Sn (< 10^{-6}), showing that these elements are highly accumulated in the intracellular medium. They may illustrate the role of metalloproteins and co-factors on the element partitioning. Indeed, molybdenum is contained in proteins enabling denitrification and cell respiration in AMB-1, and is essential for maintaining chemical conditions allowing magnetite precipitation[22,43]. This is illustrated by molybdenum-starving conditions, which severely hamper magnetite formation in AMB-1 [43]. In addition, the capacity of AMB-1 to hyper-accumulate selenium in the intracellular medium has also been reported [44]. Selenium is also involved in aerotolerance and prevents accumulation of reactive oxygen species, which helps stabilizing the gene clusters necessary for magnetosome formation [45,46]. Finally, tin is the more concentrated element in the equivalent solution. The mechanisms leading to such incorporation remain unclear, but could correspond to detoxification processes as previously proposed [47]. Alternatively, a low-affinity transporter of iron and zinc in yeast was shown to lead to tin accumulation in the intracellular medium [48]. Tin accumulation in the equivalent solution could thus represent a by-product of iron incorporation by MTB. (iii) The ratio is between 0.1 and 10, which indicates either a control by almost free diffusion between the external medium and the equivalent solution or some compensation

between transport at the cell/external medium and intracellular medium/magnetite interfaces, respectively. This third case is observed for Ag, Al, Bi, B, Cd, Ce, Cr, K, Li, Ni, Sb, Ti, U, V. Iron belongs to this category: it is not dramatically concentrated in the intracellular medium (~1.8×10^4 to 6.1×10^4 ppb *versus* 1.3×10^4 ppb in the residual growth medium), in agreement with literature data suggesting a concentration factor of the order of 3-4 in iron limited culture conditions [see below and [17]]. Overall, the present methodology is the only available approach enabling the comparison of gradients of elemental concentrations between the intracellular medium and the external aqueous solution that reveals active transfers of elements in a quantitative manner.

Modeling incorporation of divalent elements from the first transition series into magnetite

Because of lacking thermodynamic data, it is generally not possible to model the composition of magnetite at equilibrium with an aqueous solution of known composition. However, due to available data in thermodynamic databases, this can be achieved in the case of divalent elements from the first series of transition metals (X^{2+} = Mn^{2+}, Co^{2+}, Ni^{2+}, Cu^{2+}, Zn^{2+}). The mixing of a compound $X^{2+}Fe_2O_4$ in magnetite can reasonably be considered as not too far from ideality especially at low concentrations of element X in $X^{2+}Fe_2O_4$. In the case of divalent cations exchange with Fe^{2+}, reaction [1] is written as:

$$X^{2+} + Fe^{2+}Fe_2O_4 \rightleftharpoons Fe^{2+} + X^{2+}Fe_2O_4 \qquad [10]$$

The corresponding partition coefficient ($D^{X/Fe}$) of an element X normalized to iron is given by:

$$D^{X/Fe} = \frac{\{X^{2+}_{magnetite}\}\{Fe^{2+}_{solution}\}}{\{X^{2+}_{solution}\}\{Fe^{2+}_{magnetite}\}} = \frac{\left[X^{2+}_{magnetite}\right]\left[Fe^{2+}_{solution}\right]}{\left[X^{2+}_{solution}\right]} \quad [11]$$

Partition coefficients $D^{X/Fe}$ of the first series of transition elements under the assumption of ideal behavior are given in Table 3 with concentrations in solutions ($[X^{2+}_{solution}]$ and $[Fe^{2+}_{solution}]$) expressed in molalities and those in solid phase ($\left[X^{2+}_{magnetite}\right]$) in molar fractions. For abiotic magnetite precipitation, measured values of $\log D^{X/Fe}$ of Mn^{2+}, Co^{2+}, Ni^{2+}, Cu^{2+}, Zn^{2+} show similar values close to -11, ranging between -12.38 ± 0.59 (Zn) and -10.41 ± 0.01 (Mn) (Table 3), in good agreement with experimental results. Calculated values from the THERMODEM database compiled by the French Geological Survey (BRGM institute) [25] also given in Table 3 are close to these values, showing that ideal behavior upon X^{2+}-Fe^{2+} substitution is a valid assumption at least in the case of these elements. Only cobalt shows a significant discrepancy between thermodynamically-calculated (-0.8) and experimentally determined (-10.42 ± 0.19) $\log D^{X/Fe}$ values (Table 3). In the present experiment, the value obtained for cobalt (-10.42) is close to those of the other divalent elements, which is indeed the expected behavior. The origin of the very high $\log D^{X/Fe}$ value previously proposed in the case of cobalt remains unknown, but could arise from highly non-ideal behavior of cobalt solid solution in magnetite. Overall, putting aside the case of cobalt that is still uncertain, the consistency between values deduced from thermodynamic databases and assessments of partition coefficients between abiotic magnetite and the residual aqueous solution suggests that the hypothesis of local

thermodynamic equilibrium for the incorporation of trace and minor elements in magnetite is valid.

Dependence of magnetite solubility upon pH and Eh

We have measured intracellular iron concentrations to give an estimate of the iron concentration in the equivalent solution (~1.8×10^4 to 6.1×10^4 ppb), which was needed to estimate the concentration of all other chemical elements in the equivalent solution. At thermodynamic equilibrium, such iron content strongly depends on pH and Eh conditions. It is thus important to check whether pH and Eh values compatible with our iron measurements are not unrealistic from conditions typical of intracellular environments. The dissolution of magnetite can be written as:

$$Fe_3O_4 + 8H^+ \rightleftharpoons 2Fe^{3+}_{solution} + Fe^{2+}_{solution} + 4H_2O \quad [12]$$

The equilibrium constant (K_s) associated with Eq. 12 is:

$$K_s = \frac{\{Fe^{3+}_{solution}\}^2 \{Fe^{2+}_{solution}\}}{\{Fe_3O_4\}\{H^+\}^8} = \frac{[Fe^{3+}_{solution}]^2 [Fe^{2+}_{solution}]}{[H^+]^8} \quad [13]$$

with $\{Fe^{2+}_{solution}\}$ and $\{Fe^{3+}_{solution}\}$ the activities of Fe^{2+} and Fe^{3+} in the aqueous solution, respectively, $\{Fe_3O_4\}$ the activity of magnetite, and $[Fe^{2+}]_{solution}$ and $[Fe^{3+}]_{solution}$ the concentrations of Fe^{2+} and Fe^{3+} in the aqueous solution and $[H^+]$ the concentration of H^+ in solution. Magnetite activity ($\{Fe_3O_4\}$) is taken as 1 (single-component pure solid phase). As shown by Eqs. 12 and 13, the concentration of iron in solution ($Fe_{solution}$) increases when

pH decreases. If one decreases the Eh value of the equivalent solution, the Fe^{2+} content in the equivalent aqueous solution will be altered according to:

$$Fe_3O_4 + 8H^+ + 2e^- \rightleftharpoons 3Fe^{2+}_{solution} + 4H_2O \qquad [14]$$

In this case, the Fe^{2+}, Fe^{3+} and total dissolved concentrations can be determined using the redox potential (Eh) of the solution according to the Nernst equation:

$$Eh = E_0 + \left(\frac{RT}{nF}\right) \mathrm{Ln} \left(\frac{\{Fe_3O_4\}\{H^+\}^8}{\{Fe^{2+}_{solution}\}^3}\right) = E_0 + \left(\frac{RT}{nF}\right) \mathrm{Ln} \left(\frac{\{Fe_3O_4\}[H^+]^8}{[Fe^{2+}_{solution}]^3}\right) \qquad [15]$$

where E_0 is the standard potential, R is the ideal gas constant, T is the temperature in Kelvin, n is the number of electrons transferred in the reaction, and F is the Faraday constant. The concentration $[Fe^{2+}_{solution}]$ thus increases when Eh decreases. Using Eqs. 12 and 15, the concentration of Fe^{2+} and of total dissolved iron released by magnetite dissolution were calculated for each pH and Eh values using the CHESS code (see materials and methods). Results are shown in Fig. 3A.

Abiotic magnetite was synthesized under known pH (12) and Eh (-0.75 V) conditions [49]. The decimal logarithm of the concentration in residual iron ($\log[Fe^{2+}]$ in molar) was measured (-7.09, see Table S1). Under these pH and Eh conditions, all free iron is calculated to be Fe^{2+} (Fig. S1). As illustrated in Fig. 3A, the $\log[Fe^{2+}]$ calculated in the solution at equilibrium with magnetite at a pH of 12 and a Eh of -0.75 V is -7.25, which is close to the measured value of -7.09. These pH and Eh conditions also fall in the magnetite stability domain (Fig. 2), and are thus consistent with the preferential precipitation of magnetite as the stable iron-bearing phase.

The agreement between measured iron concentrations in contact with magnetite at pH 12 and Eh of -0.75 V is also consistent with the hypothesis of thermodynamic equilibrium and validates our modelling approach.

The same methodology was then applied to infer the pH and Eh conditions in the equivalent solution, which is possible thanks to the estimates of intracellular dissolved iron concentrations (Tables 1 and 2) ranging between $3.25 \pm 1.53 \times 10^{-4}$ and $1.09 \pm 0.51 \times 10^{-3}$ M ($\log[Fe^{2+}]$ values of -3.48 and -2.96, respectively). Only free Fe^{2+} was considered in those calculations (Fig. 3A), which may not be an accurate description of dissolved iron in the cell environment [35]. We thus investigated the impact of iron complexation by ligands (L^{2-}) on the modeling of magnetite solubility and associated release of Fe^{2+}. Two ligands showing different affinity constants (β) with Fe^{2+} were considered given by:

$$\beta = \frac{[FeL]}{[Fe^{2+}]\,[L^{2-}]} \qquad [16]$$

Magnetite solubility was calculated in the presence of two ligands with affinity constants of $\log\beta = 5$ and 10, respectively (Fig. 3B and 3C). Results show that the presence of ligands increases magnetite solubility, with higher concentrations of dissolved Fe^{2+} for given pH and Eh values. Increased magnetite solubility was more pronounced for higher logβ. It was already shown that dissolved Fe^{2+} in MTB is associated with phosphates [35], which have a logβ of 3.6 for complexation with Fe^{2+} [50]. Labile Fe^{2+} was also identified in MTB [37]. Therefore, a logβ higher than 5 for complexation with Fe^{2+} may not be realistic. The range of pH and Eh values of the equivalent solution is then deduced from Fig. 3B and shown more precisely in Fig. 4. The pH and Eh values of the equivalent solution are estimated to be comprised in the ranges

7.5 – 9 and -0.25 V – -0.6 V, respectively, centered near pH = 8.5 and Eh = -0.45 V for falling within the primary stability field of magnetite (Figs. 2 and 4). Almost all Fe^{2+} (93 %) is then associated with its ligand (L^{2-}) (Fig. S2), supporting the results of previous experiments [34,35]. Iron in the equivalent solution is also present as Fe^{2+} under these conditions (Fig. S1), in good agreement with experimental observations [34,35,37].

The meaning of the equivalent solution

The present work establishes the concentrations in trace and minor elements as well as the pH and Eh of the equivalent solution, which is defined as the aqueous solution at thermodynamic equilibrium with magnetite. This leaves open the question of the interpretation of the equivalent solution. The elemental content, pH and Eh of the equivalent solution have been reconstructed based on the iron concentration in the cytoplasm. Thus, the dissolved Fe(II) concentration was considered to be homogeneous so that the chemical properties of the equivalent solution in contact with magnetite is assumed not to be dramatically different from the bulk intracellular medium. Such picture is supported by the fluorescent detection of labile Fe(II) in AMB-1 homogenously distributed in the cell [37]. However, some AMB-1 cells accumulated labile Fe(II) at the location of both magnetite-containing and magnetite-free magnetosome vesicles [37]. At this stage, we cannot firmly determine whether the equivalent solution is more representative of the cytoplasmic environment or of more local compartments (magnetosome organelles). The range of pH values (7.5 - 9.5) compatible with the experimentally-determined magnetite solubility and shown in Fig. 4 demonstrates sub-basic to basic conditions in the equivalent solution, which is close to or higher than the one proposed for AMB-1 cytoplasm (~7.5) [51]. A more precise

and direct measurement of pH conditions within magnetosomes [such as what has been initiated using fluorescent constructions in prokaryotes [51], although the precise location of the fluorescent reporters could not be checked due to the limitations mentioned in the introduction, and in eukaryotes [10–12]] could, if coupled to measurements of iron in the same vesicles, lead to more precise scenarios in terms of redox and iron speciation inside these organelles.

Conclusions

From a combination of experimental and modeling approaches, we were able to determine the elemental composition, pH and Eh of an hypothetical solution being in contact with magnetite nanoparticles produced by MTB in their magnetosomes. We identified strong elemental gradients between the intracellular and extracellular media, leading to efflux processes or active pumping of trace elements into bacteria. The pH and Eh conditions in the equivalent solution inferred from the presented methodology fall within the magnetite stability domain and are thus consistent with the preferential magnetite precipitation in magnetosomes. Future application of the methodology presented in this work to distinct bacterial organelles will deepen our understanding of key biological functions in prokaryotic microorganisms. A notable example of such intracellular inclusions correspond to calcium-carbonate vesicles in cyanobacteria and MTB, which were shown to be formed in a genetically controlled manner within membrane-delimited vesicles [52,53]. Precipitation of calcium carbonates requires higher pH than that of cytoplasmic environments [54], suggesting a regulated pH in the carbonate-forming vesicles and pointing to a potential organelle function of these vesicles. This hypothesis could be tested using the methodology presented here.

Associated content

Supporting Information

Figure S1. Fe^{2+}/ total Fe ratios under various pH/Eh conditions in solutions containing no ligand, or containing iron ligands with stability constants (logβ) of 5 or 10.

Figure S2. Complexation of dissolved Fe(II) by ligands (L) with complexation constants (logβ) of 5 and 10, and under various pH/Eh conditions.

Table S1. Mass concentrations of trace and minor elements in magnetite and residual solution, and measured partition coefficients in the case of abiotic precipitation of magnetite.

Table S2. Mass concentrations of trace and minor elements in magnetite and residual solution in the case of biological magnetite.

Table S3. Mass of iron per AMB-1 cell and intracellular bulk iron concentration measured with single-cell – inductively coupled plasma – mass spectrometry in bacterial cultures supplemented with Fe(III)-citrate at 10, 50, 100, 200, 300 and 500 μM.

Table S4. Mass concentration of trace and minor elements in the residual growth medium, ratios of concentrations in the residual growth medium versus concentrations in the equivalent solution, and concentrations of trace and minor elements in magnetite and residual growth medium normalized to iron.

Acknowledgements

MA is supported by a grant through the *Fondation pour la Recherche Médicale* (ARF201909009123). DF is supported by the *Commissariat à l'énergie atomique et aux énergies alternatives*. This work was supported by the French National Research Agency (project SIGMAG: ANR-18-CE31-0003). Part of this work was supported by IPGP

multidisciplinary program PARI and by Region Île-de-France SESAME Grant no. 12015908.

References

(1) Kartal, B.; van Niftrik, L.; Keltjens, J. T.; Op den Camp, H. J. M.; Jetten, M. S. M. Anammox--Growth Physiology, Cell Biology, and Metabolism. *Adv. Microb. Physiol.* **2012**, *60*, 211–262. https://doi.org/10.1016/B978-0-12-398264-3.00003-6.

(2) Seufferheld, M.; Vieira, M. C. F.; Ruiz, F. A.; Rodrigues, C. O.; Moreno, S. N. J.; Docampo, R. Identification of Organelles in Bacteria Similar to Acidocalcisomes of Unicellular Eukaryotes. *J. Biol. Chem.* **2003**, *278* (32), 29971–29978. https://doi.org/10.1074/jbc.M304548200.

(3) Grant, C. R.; Wan, J.; Komeili, A. Organelle Formation in Bacteria and Archaea. In *Annual Review of Cell and Developmental Biology, Vol 34*; Lehmann, R., Ed.; Annual Reviews: Palo Alto, 2018; Vol. 34, pp 217–238.

(4) Burgener, S.; Luo, S.; McLean, R.; Miller, T. E.; Erb, T. J. A Roadmap towards Integrated Catalytic Systems of the Future. *Nat Catal* **2020**, *3* (3), 186–192. https://doi.org/10.1038/s41929-020-0429-x.

(5) Siedlik, M. J.; Yang, Z.; Kadam, P. S.; Eberwine, J.; Issadore, D. Micro- and Nano-Devices for Studying Subcellular Biology. *Small* **2021**, *17* (3), 2005793. https://doi.org/10.1002/smll.202005793.

(6) Bentov, S.; Brownlee, C.; Erez, J. The Role of Seawater Endocytosis in the Biomineralization Process in Calcareous Foraminifera. *PNAS* **2009**, *106* (51), 21500–21504. https://doi.org/10.1073/pnas.0906636106.

(7) Wu, M. M.; Llopis, J.; Adams, S.; McCaffery, J. M.; Kulomaa, M. S.; Machen, T. E.; Moore, H.-P. H.; Tsien, R. Y. Organelle PH Studies Using Targeted Avidin and Fluorescein–Biotin. *Chemistry & Biology* **2000**, *7* (3), 197–209. https://doi.org/10.1016/S1074-5521(00)00088-0.

(8) Shen, J.; Zeng, Y.; Zhuang, X.; Sun, L.; Yao, X.; Pimpl, P.; Jiang, L. Organelle PH in the Arabidopsis Endomembrane System. *Molecular Plant* **2013**, *6* (5), 1419–1437. https://doi.org/10.1093/mp/sst079.

(9) Breckwoldt, M. O.; Armoundas, A. A.; Aon, M. A.; Bendszus, M.; O'Rourke, B.; Schwarzländer, M.; Dick, T. P.; Kurz, F. T. Mitochondrial Redox and PH Signaling Occurs in Axonal and Synaptic Organelle Clusters. *Scientific Reports* **2016**, *6* (1), 23251. https://doi.org/10.1038/srep23251.

(10) Vidavsky, N.; Addadi, S.; Mahamid, J.; Shimoni, E.; Ben-Ezra, D.; Shpigel, M.; Weiner, S.; Addadi, L. Initial Stages of Calcium Uptake and Mineral Deposition in Sea Urchin Embryos. *PNAS* **2014**, *111* (1), 39–44. https://doi.org/10.1073/pnas.1312833110.

(11) Vidavsky, N.; Masic, A.; Schertel, A.; Weiner, S.; Addadi, L. Mineral-Bearing Vesicle Transport in Sea Urchin Embryos. *Journal of Structural Biology* **2015**, *192* (3), 358–365. https://doi.org/10.1016/j.jsb.2015.09.017.

(12) Jantschke, A.; Pinkas, I.; Schertel, A.; Addadi, L.; Weiner, S. Biomineralization Pathways in Calcifying Dinoflagellates: Uptake, Storage in MgCaP-Rich Bodies and Formation of the Shell. *Acta Biomaterialia* **2020**, *102*, 427–439. https://doi.org/10.1016/j.actbio.2019.11.042.

(13) Uebe, R.; Schueler, D. Magnetosome Biogenesis in Magnetotactic Bacteria. *Nat. Rev. Microbiol.* **2016**, *14* (10), 621–637. https://doi.org/10.1038/nrmicro.2016.99.

(14) Frankel, R.; Blakemore, R.; Dearaujo, F.; Esquivel, D.; Danon, J. Magnetotactic Bacteria at the Geomagnetic Equator. *Science* **1981**, *212* (4500), 1269–1270.

https://doi.org/10.1126/science.212.4500.1269.
(15) Murat, D.; Quinlan, A.; Vali, H.; Komeili, A. Comprehensive Genetic Dissection of the Magnetosome Gene Island Reveals the Step-Wise Assembly of a Prokaryotic Organelle. *Proc. Natl. Acad. Sci. U. S. A.* **2010**, *107* (12), 5593–5598. https://doi.org/10.1073/pnas.0914439107.
(16) Komeili, A.; Li, Z.; Newman, D. K.; Jensen, G. J. Magnetosomes Are Cell Membrane Invaginations Organized by the Actin-like Protein MamK. *Science* **2006**, *311* (5758), 242–245. https://doi.org/10.1126/science.1123231.
(17) Amor, M.; Tharaud, M.; Gélabert, A.; Komeili, A. Single-Cell Determination of Iron Content in Magnetotactic Bacteria: Implications for the Iron Biogeochemical Cycle. *Environ. Microbiol.* **2020**, *22* (3), 823–831. https://doi.org/10.1111/1462-2920.14708.
(18) Amor, M.; Busigny, V.; Louvat, P.; Tharaud, M.; Gélabert, A.; Cartigny, P.; Carlut, J.; Isambert, A.; Durand-Dubief, M.; Ona-Nguema, G. *et al*. Iron Uptake and Magnetite Biomineralization in the Magnetotactic Bacterium Magnetospirillum Magneticum Strain AMB-1: An Iron Isotope Study. *Geochim. Cosmochim. Acta* **2018**, *232*, 225–243. https://doi.org/10.1016/j.gca.2018.04.020.
(19) Addadi, L.; Gal, A.; Faivre, D.; Scheffel, A.; Weiner, S. Control of Biogenic Nanocrystal Formation in Biomineralization. *Israel Journal of Chemistry* **2016**, *56* (4), 227–241. https://doi.org/10.1002/ijch.201500038.
(20) Cornejo, E.; Subramanian, P.; Li, Z.; Jensen, G. J.; Komeili, A. Dynamic Remodeling of the Magnetosome Membrane Is Triggered by the Initiation of Biomineralization. *mBio* **2016**, *7* (1), e01898-15. https://doi.org/10.1128/mBio.01898-15.
(21) Wan, J.; Browne, P. J.; Hershey, D. M.; Montabana, E.; Iavarone, A. T.; Downing, K. H.; Komeili, A. A Protease-Mediated Switch Regulates the Growth of Magnetosome Organelles in Magnetospirillum Magneticum. *Proc. Natl. Acad. Sci. U. S. A.* **2022**, *119* (6). https://doi.org/10.1073/pnas.2111745119.
(22) Amor, M.; Busigny, V.; Durand-Dubief, M.; Tharaud, M.; Ona-Nguema, G.; Gélabert, A.; Alphandéry, E.; Menguy, N.; Benedetti, M. F.; Chebbi, I. *et al*. Chemical Signature of Magnetotactic Bacteria. *Proc. Natl. Acad. Sci. U. S. A.* **2015**, *112* (6), 1699–1703. https://doi.org/10.1073/pnas.1414112112.
(23) Tharaud, M.; Gardoll, S.; Khelifi, O.; Benedetti, M. F.; Sivry, Y. UFREASI: User-FRiendly Elemental DAta ProcesSIng. A Free and Easy-to-Use Tool for Elemental Data Treatment. *Microchem J.* **2015**, *121*, 32–40. https://doi.org/10.1016/j.microc.2015.01.011.
(24) Van der Lee, J.; De Windt, L. CHESS Tutorial and Cookbook. Updated for Version 3.0, Manual Nr. LHM/RD/02/13.; Paris, 2002; p 116.
(25) Blanc, P.; Lassin, A.; Piantone, P.; Azaroual, M.; Jacquemet, M.; Fabbri, A.; Gaucher, E. C. Thermoddem: A Geochemical Database Focused on Low Temperature Water/Rock Interactions and Waste Materials. *Appl. Geochem.* **2012**, *27* (10), 2107–2116. https://doi.org/10.1016/j.apgeochem.2012.06.002.
(26) Liang, X.; Zhong, Y.; Zhu, S.; He, H.; Yuan, P.; Zhu, J.; Jiang, Z. The Valence and Site Occupancy of Substituting Metals in Magnetite Spinel Structure Fe3−xMxO4 (M = Cr, Mn, Co and Ni) and Their Influence on Thermal Stability: An XANES and TG-DSC Investigation. *Solid State Sci.* **2013**, *15*, 115–122. https://doi.org/10.1016/j.solidstatesciences.2012.10.005.
(27) Prozorov, T.; Perez-Gonzalez, T.; Valverde-Tercedor, C.; Jimenez-Lopez, C.;

Yebra-Rodriguez, A.; Körnig, A.; Faivre, D.; Mallapragada, S. K.; Howse, P. A.; Bazylinski, D. A. *et al*. Manganese Incorporation into the Magnetosome Magnetite: Magnetic Signature of Doping. *Eur. J. Mineral.* **2014**, *26* (4), 457–471. https://doi.org/10.1127/0935-1221/2014/0026-2388.
(28) Marcano, L.; Muñoz, D.; Martín-Rodríguez, R.; Orue, I.; Alonso, J.; García-Prieto, A.; Serrano, A.; Valencia, S.; Abrudan, R.; Fernández Barquín, L. *et al.* Magnetic Study of Co-Doped Magnetosome Chains. *J. Phys. Chem. C* **2018**, *122* (13), 7541–7550. https://doi.org/10.1021/acs.jpcc.8b01187.
(29) Staniland, S.; Williams, W.; Telling, N.; Van der Laan, G.; Harrison, A.; Ward, B. Controlled Cobalt Doping of Magnetosomes in Vivo. *Nat. Nanotechnol.* **2008**, *3* (3), 158–162. https://doi.org/10.1038/nnano.2008.35.
(30) Schuler, D.; Baeuerlein, E. Dynamics of Iron Uptake and Fe3O4 Biomineralization during Aerobic and Microaerobic Growth of Magnetospirillum Gryphiswaldense. *J. Bacteriol.* **1998**, *180* (1), 159–162.
(31) Heyen, U.; Schuler, D. Growth and Magnetosome Formation by Microaerophilic Magnetospirillum Strains in an Oxygen-Controlled Fermentor. *Appl. Microbiol. Biotechnol.* **2003**, *61* (5–6), 536–544. https://doi.org/10.1007/s00253-002-1219-x.
(32) Olszewska-Widdrat, A.; Schiro, G.; Reichel, V. E.; Faivre, D. Reducing Conditions Favor Magnetosome Production in Magnetospirillum Magneticum AMB-1. *Front. Microbiol.* **2019**, *10*, 582. https://doi.org/10.3389/fmicb.2019.00582.
(33) Loferer-Krößbacher, M.; Klima, J.; Psenner, R. Determination of Bacterial Cell Dry Mass by Transmission Electron Microscopy and Densitometric Image Analysis. *Appl. Environ. Microbiol.* **1998**, *64* (2), 688–694. https://doi.org/10.1128/AEM.64.2.688-694.1998.
(34) Faivre, D.; Boettger, L. H.; Matzanke, B. F.; Schueler, D. Intracellular Magnetite Biomineralization in Bacteria Proceeds by a Distinct Pathway Involving Membrane-Bound Ferritin and an Iron(II) Species. *Angew. Chem.-Int. Edit.* **2007**, *46* (44), 8495–8499. https://doi.org/10.1002/anie.200700927.
(35) Uebe, R.; Ahrens, F.; Stang, J.; Jäger, K.; Böttger, L. H.; Schmidt, C.; Matzanke, B. F.; Schüler, D. Bacterioferritin of Magnetospirillum Gryphiswaldense Is a Heterotetraeicosameric Complex Composed of Functionally Distinct Subunits but Is Not Involved in Magnetite Biomineralization. *mBio* **2019**, *10* (3). https://doi.org/10.1128/mBio.02795-18.
(36) Frankel, R.; Papaefthymiou, G.; Blakemore, R.; Obrien, W. Fe_3O_4 Precipitation in Magnetotactic Bacteria. *Biochimica Et Biophysica Acta* **1983**, *763* (2), 147–159. https://doi.org/10.1016/0167-4889(83)90038-1.
(37) Amor, M.; Ceballos, A.; Wan, J.; Simon, C. P.; Aron, A. T.; Chang, C. J.; Hellman, F.; Komeili, A. Magnetotactic Bacteria Accumulate a Large Pool of Iron Distinct from Their Magnetite Crystals. *Appl. Environ. Microbiol.* **2020**, *86* (22). https://doi.org/10.1128/AEM.01278-20.
(38) Baumgartner, J.; Morin, G.; Menguy, N.; Gonzalez, T. P.; Widdrat, M.; Cosmidis, J.; Faivre, D. Magnetotactic Bacteria Form Magnetite from a Phosphate-Rich Ferric Hydroxide via Nanometric Ferric (Oxyhydr)Oxide Intermediates. *Proc. Natl. Acad. Sci. U. S. A.* **2013**, *110* (37), 14883–14888. https://doi.org/10.1073/pnas.1307119110.
(39) Fdez-Gubieda, L. M.; Muela, A.; Alonso, J.; Garcia-Prieto, A.; Olivi, L.; Fernandez-Pacheco, R.; Manuel Barandiaran, J. Magnetite Biomineralization in

Magnetospirillum Gryphiswaldense: Time-Resolved Magnetic and Structural Studies. *ACS Nano* **2013**, *7* (4), 3297–3305. https://doi.org/10.1021/nn3059983.
(40) Suzuki, T.; Okamura, Y.; Calugay, R. J.; Takeyama, H.; Matsunaga, T. Global Gene Expression Analysis of Iron-Inducible Genes in Magnetospirillum Magneticum AMB-1. *J. Bacteriol.* **2006**, *188* (6), 2275–2279. https://doi.org/10.1128/JB.188.6.2275-2279.2006.
(41) Klein, J. S.; Lewinson, O. Bacterial ATP-Driven Transporters of Transition Metals: Physiological Roles, Mechanisms of Action, and Roles in Bacterial Virulence. *Metallomics* **2011**, *3* (11), 1098–1108. https://doi.org/10.1039/c1mt00073j.
(42) Corradino, R. A.; Ebel, J. G.; Craig, P. H.; Taylor, A. N.; Wasserman, R. H. Calcium Absorption and the Vitamin D3-Dependent Calcium-Binding Protein. *Calc. Tis Res.* **1971**, *7* (1), 81–92. https://doi.org/10.1007/BF02062596.
(43) Taoka, A.; Yoshimatsu, K.; Kanemori, M.; Fukumori, Y. Nitrate Reductase from the Magnetotactic Bacterium Magnetospirillum Magnetotacticum MS-1: Purification and Sequence Analyses. *Can. J. Microbiol.* **2003**, *49* (3), 197–206. https://doi.org/10.1139/W03-028.
(44) Tanaka, M.; Knowles, W.; Brown, R.; Hondow, N.; Arakaki, A.; Baldwin, S.; Staniland, S.; Matsunaga, T. Biomagnetic Recovery and Bioaccumulation of Selenium Granules in Magnetotactic Bacteria. *Appl. Environ. Microbiol.* **2016**, *82* (13), 3886–3891. https://doi.org/10.1128/AEM.00508-16.
(45) Rotruck, J. T.; Pope, A. L.; Ganther, H. E.; Swanson, A. B.; Hafeman, D. G.; Hoekstra, W. G. Selenium: Biochemical Role as a Component of Glutathione Peroxidase. *Science* **1973**, *179* (4073), 588–590. https://doi.org/10.1126/science.179.4073.588.
(46) Ge, X.; Wang, K.; Bo, T.; Kou, Y.; Liu, W.; Chen, G. Magnetospirillum Magneticum AMB-1 Peroxiredoxins Contribute to the Aerotolerance and Genetic Stability of the Genomic Magnetosome Island. *FEMS Microbiol. Lett.* **2011**, *320* (2), 118–127. https://doi.org/10.1111/j.1574-6968.2011.02298.x.
(47) Komeili, A. Molecular Mechanisms of Compartmentalization and Biomineralization in Magnetotactic Bacteria. *Fems Microbiol. Rev.* **2012**, *36* (1), 232–255. https://doi.org/10.1111/j.1574-6976.2011.00315.x.
(48) Viau, C. M.; Cardone, J. M.; Guecheva, T. N.; Yoneama, M.-L.; Dias, J. F.; Pungartnik, C.; Brendel, M.; Saffi, J.; Henriques, J. A. P. Enhanced Resistance of Yeast Mutants Deficient in Low-Affinity Iron and Zinc Transporters to Stannous-Induced Toxicity. *Chemosphere* **2012**, *86* (5), 477–484. https://doi.org/10.1016/j.chemosphere.2011.10.007.
(49) Ona-Nguema, G.; Morin, G.; Wang, Y.; Foster, A. L.; Juillot, F.; Calas, G.; Brown, G. E. XANES Evidence for Rapid Arsenic(III) Oxidation at Magnetite and Ferrihydrite Surfaces by Dissolved O-2 via Fe2+-Mediated Reactions. *Environ. Sci. Technol.* **2010**, *44* (14), 5416–5422. https://doi.org/10.1021/es1000616.
(50) Rauen, U.; Springer, A.; Weisheit, D.; Petrat, F.; Korth, H.-G.; de Groot, H.; Sustmann, R. Assessment of Chelatable Mitochondrial Iron by Using Mitochondrion-Selective Fluorescent Iron Indicators with Different Iron-Binding Affinities. *ChemBioChem* **2007**, *8* (3), 341–352. https://doi.org/10.1002/cbic.200600311.
(51) Eguchi, Y.; Fukumori, Y.; Taoka, A. Measuring Magnetosomal pH of the Magnetotactic Bacterium Magnetospirillum Magneticum AMB-1 Using pH-Sensitive Fluorescent Proteins. *Biosci. Biotechnol. Biochem.* **2018**, *82* (7), 1243–1251.

https://doi.org/10.1080/09168451.2018.1451739.
(52) Benzerara, K.; Skouri-Panet, F.; Li, J.; Ferard, C.; Gugger, M.; Laurent, T.; Couradeau, E.; Ragon, M.; Cosmidis, J.; Menguy, N. *et al*. Intracellular Ca-Carbonate Biomineralization Is Widespread in Cyanobacteria. *Proc. Natl. Acad. Sci. U. S. A.* **2014**, *111* (30), 10933–10938. https://doi.org/10.1073/pnas.1403510111.
(53) Monteil, C. L.; Benzerara, K.; Menguy, N.; Bidaud, C. C.; Michot-Achdjian, E.; Bolzoni, R.; Mathon, F. P.; Coutaud, M.; Alonso, B.; Garau, C. *et al*. Intracellular Amorphous Ca-Carbonate and Magnetite Biomineralization by a Magnetotactic Bacterium Affiliated to the Alphaproteobacteria. *ISME J* **2021**, *15* (1), 1–18. https://doi.org/10.1038/s41396-020-00747-3.
(54) Merz, M. U. E. The Biology of Carbonate Precipitation by Cyanobacteria. *Facies* **1992**, *26* (1), 81–101. https://doi.org/10.1007/BF02539795.
(55) Berny, C.; Le Fèvre, R.; Guyot, F.; Blondeau, K.; Guizonne, C.; Rousseau, E.; Bayan, N.; Alphandéry, E. A Method for Producing Highly Pure Magnetosomes in Large Quantity for Medical Applications Using Magnetospirillum Gryphiswaldense MSR-1 Magnetotactic Bacteria Amplified in Minimal Growth Media. *Front Bioeng Biotechnol* **2020**, *8*, 16. https://doi.org/10.3389/fbioe.2020.00016.

Figures

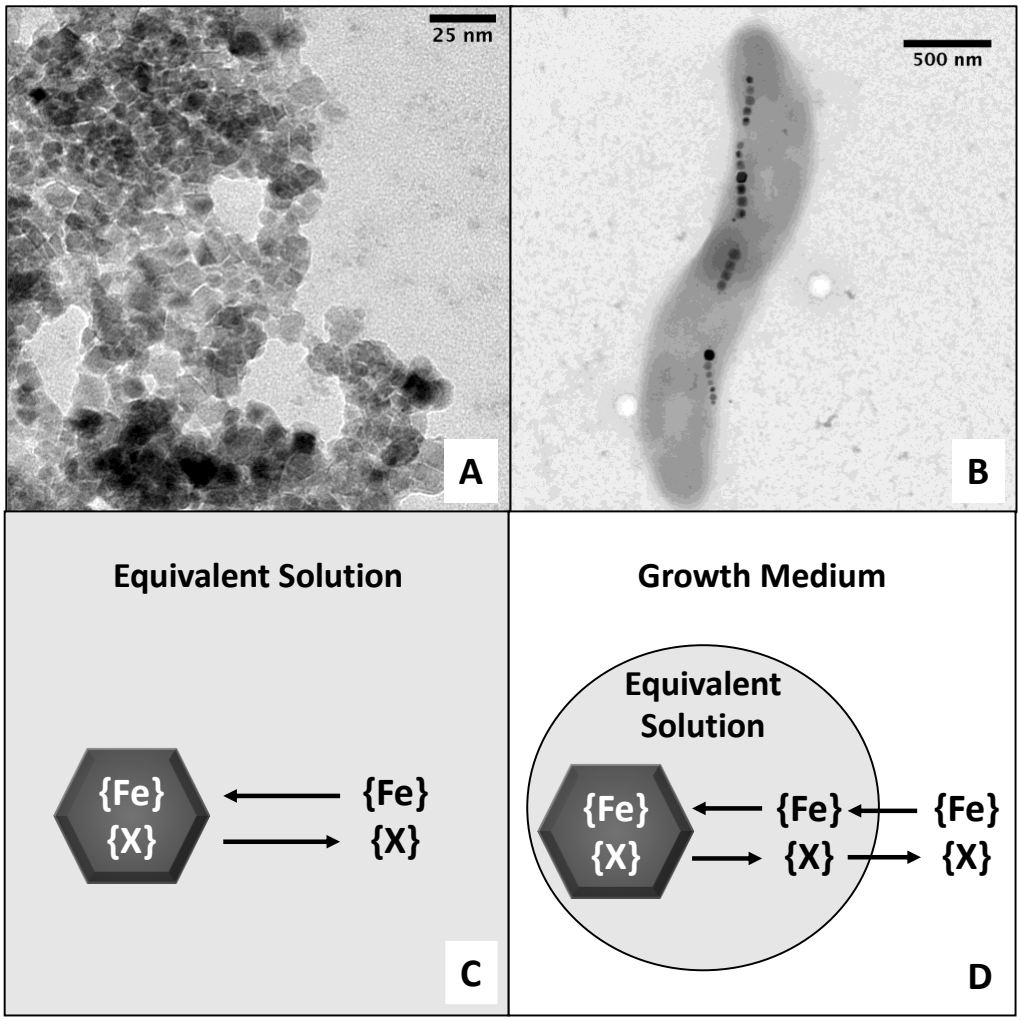

Figure 1. Transmission electron microscopy observation of (A) abiotic magnetite nanoparticles and (B) the magnetotactic strain *Magnetospirillum magneticum* AMB-1. (C-D) Fate of iron (Fe) and distinct cations (X) during (C) abiotic magnetite formation in aqueous solution and (D) in AMB-1 magnetite. Dark solids represent magnetite nanoparticles. {Fe} and {X} correspond to the activity of Fe and X, respectively, in magnetite, the equivalent solution (see main text for details) and the growth medium of MTB. They were all measured using mass spectrometry, except {Fe} and {X} values of the equivalent solution in MTB. The present work aims at determining the element composition, pH and redox potential (E_h) of the equivalent solution being at equilibrium with the biological magnetite.

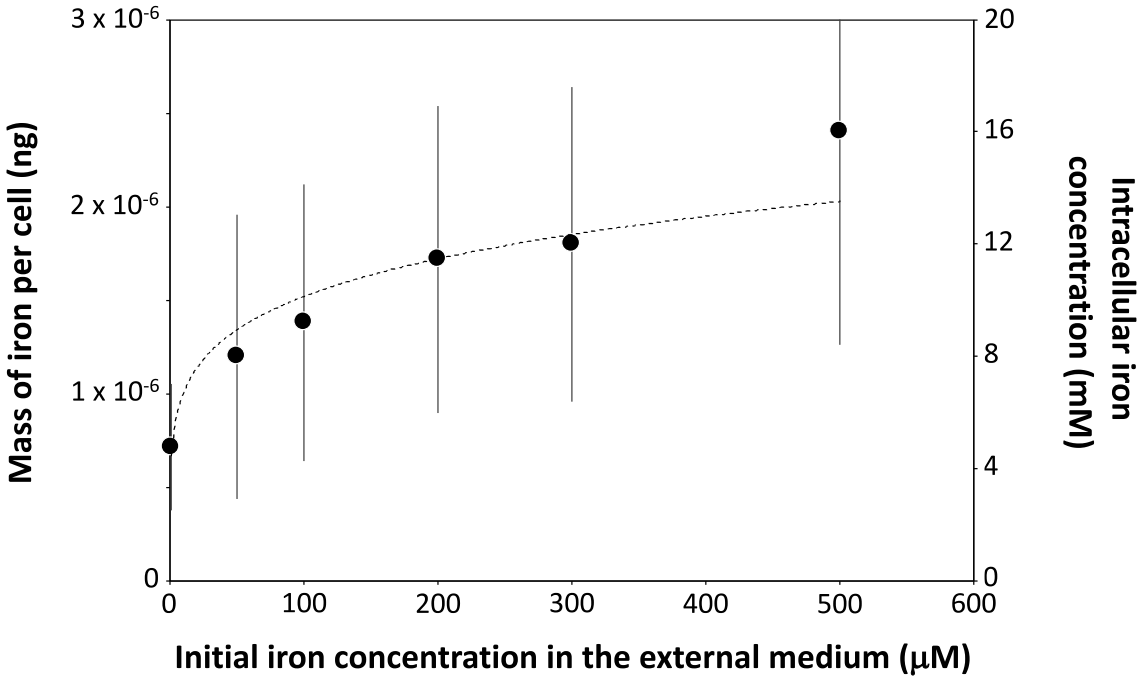

Figure 2. Mass of iron per AMB-1 cell measured with single-cell – inductively coupled plasma – mass spectrometry in bacterial cultures supplemented with Fe(III)-citrate at 10, 50, 100, 200, 300 and 500 μM. The intracellular concentration in bulk iron was calculated assuming that bacteria are 3-μm long cylinders with a radius of 0.5 μm (Fig. 1).

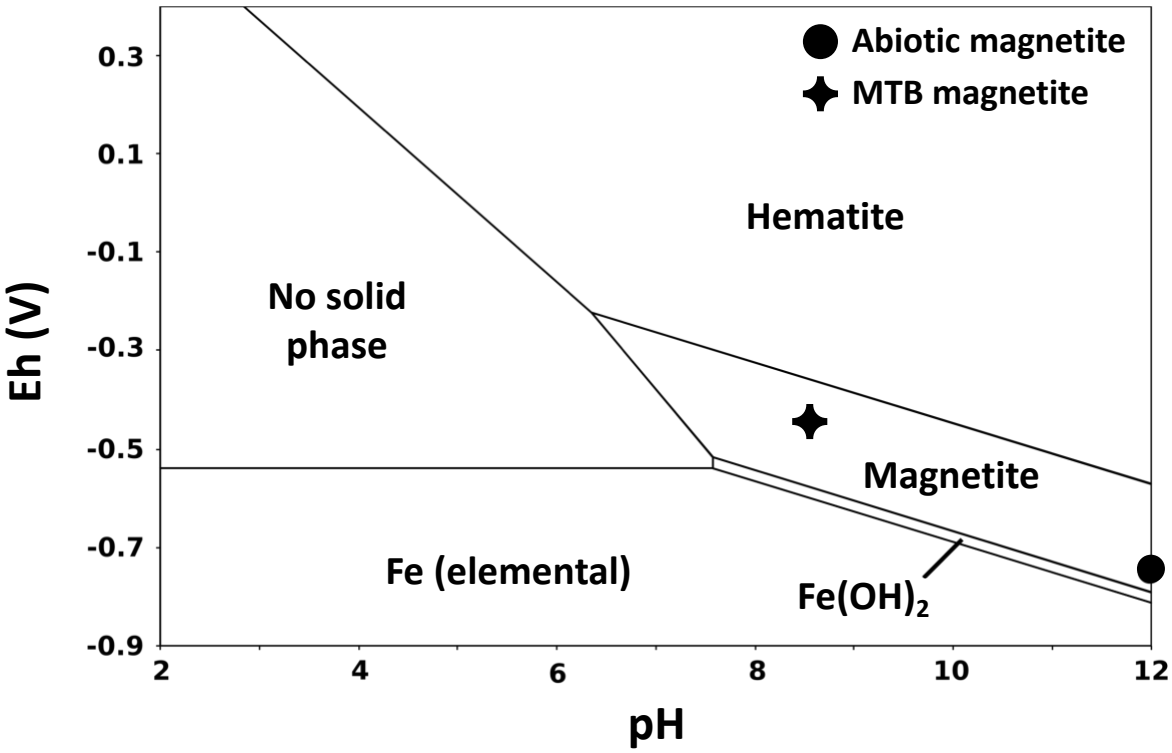

Figure 3. Stability domains of iron solid phases under a range of pH (2/12) and Eh (-0.9/0.4 V) conditions calculated with an initial dissolved magnetite concentration (5×10^{-3} M) representative of MTB (see Materials and Methods). Addition of iron ligands in the system does not affect the distribution of stability domains.

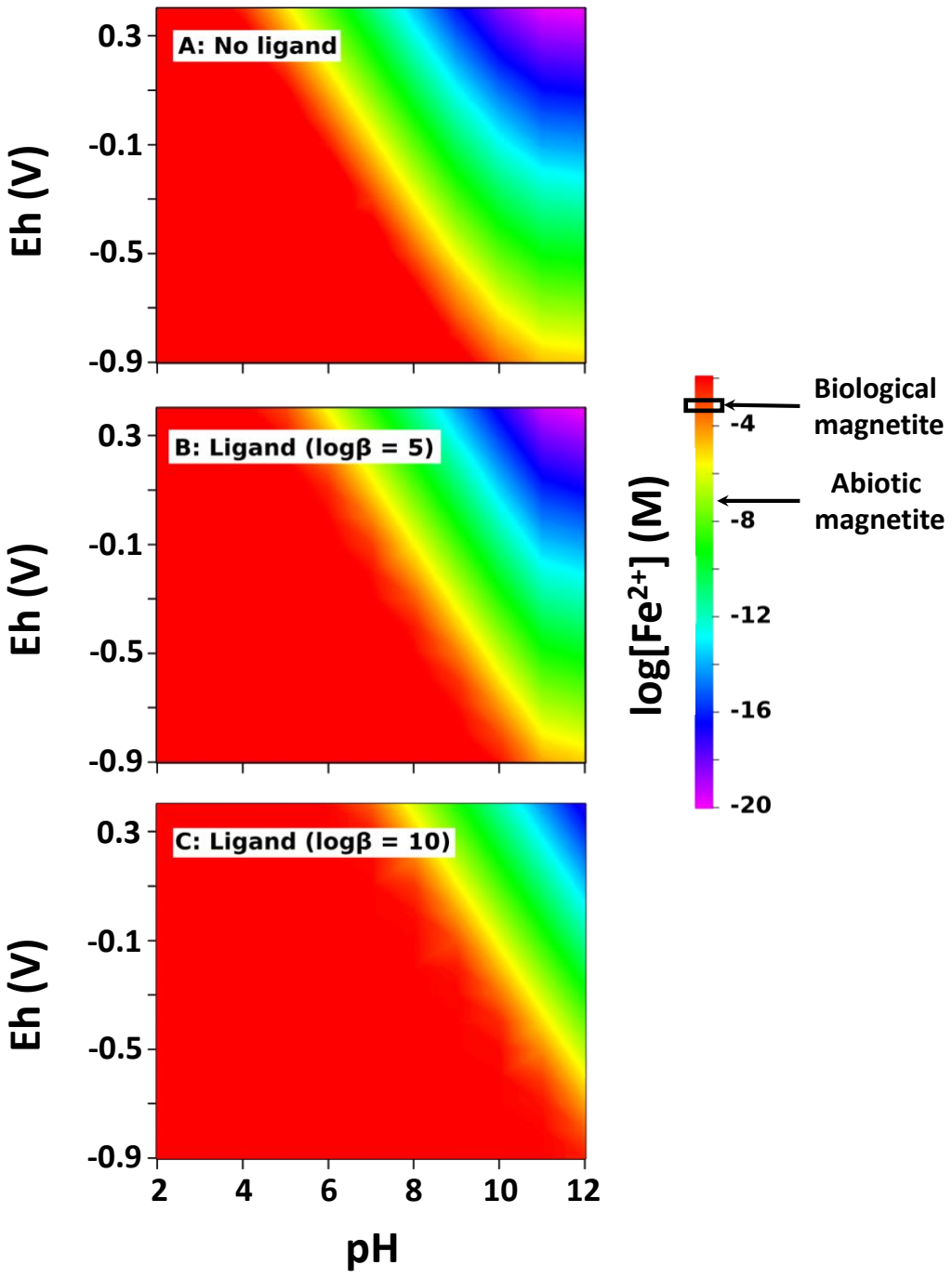

Figure 4. Modeling of magnetite solubility under various pH and Eh conditions. The concentration of Fe^{2+} (in molars) in the solution at equilibrium with magnetite was calculated and expressed as $\log[Fe^{2+}]$ in (A) the absence of iron ligands, and with ligands having various stability constants (logβ) with iron of (B) 5 and (C) 10.

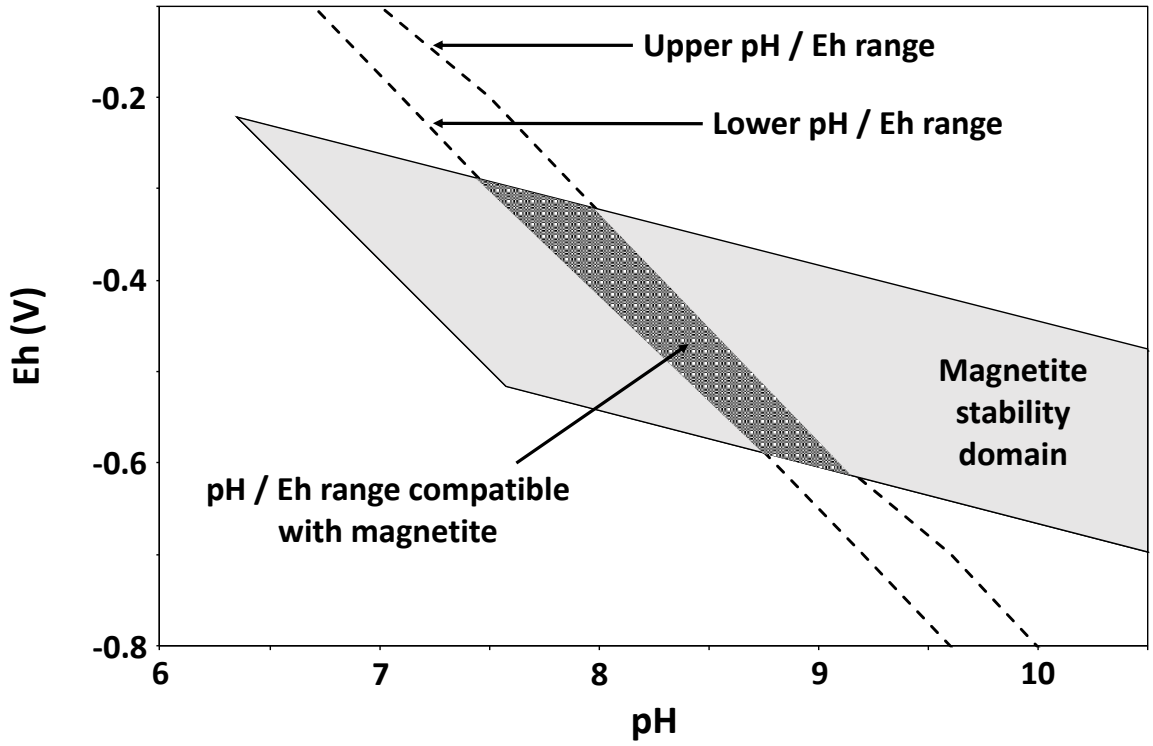

Figure 5. Range of pH / Eh (dashed lines) compatible with the iron concentration ($-3.48 < \log[Fe^{2+}] < -2.96$) and speciation (complexation with ligands having $\log\beta = 5$) in the equivalent solution for each Eh value. The magnetite stability domain (light grey area) is also reported. The filled area represents the range of pH and Eh values compatible with the presence of magnetite.

Tables

Table 1. Iron speciation in the three magnetotactic strains *Magnetospirillum magneticum* AMB-1, *Magnetospirillum gryphiswaldense* MSR-1 and *Magnetospirillum magnetotacticum* MS-1.

Reference	Strain	Fraction of iron in magnetite (%)	Fraction of iron in ferrihydrite (%)	Fraction of iron in Fe(II) (%)
[34]	MSR-1	71.7	21.9	6.4
[35]	MSR-1	61.2	22.7	6.1
[55]	MSR-1	50	0 to 50	0 to 50
[37]	AMB-1	30 to 40	0 to 70	0 to 70
[18]	AMB-1	50	0 to 50	0 to 50
[36]	MS-1	80	0 to 20	0 to 20

Table 2. Massic concentrations (in ppb) of trace and minor elements in the equivalent solution at equilibrium with biological magnetite. Each value represents the mean of fermentor (one replicate) and bottle (two replicates) cultures ± one standard deviation (SD).

Element	Concentration in equivalent solution (ppb) ±1SD	Concentration in residual growth medium (ppb) ± 1SD	[X] in the residual growth medium / [X] in the equivalent solution
Ag	$0.82 \pm 1.13 \times 10^{1}$	1.18×10^{1}	7.32×10^{-1}
Al	$6.89 \pm 9.72 \times 10^{5}$	$1.48 \pm 0.52 \times 10^{3}$	$6.20 \pm 8.75 \times 10^{-1}$
As	$3.79 \pm 1.75 \times 10^{4}$	$7.77 \pm 2.14 \times 10^{2}$	$2.45 \pm 1.70 \times 10^{-2}$
B	$4.71 \pm 4.85 \times 10^{4}$	$5.35 \pm 5.61 \times 10^{3}$	$1.11 \pm 0.05 \times 10^{-1}$
Ba	$2.26 \pm 2.62 \times 10^{1}$	$5.14 \pm 3.15 \times 10^{2}$	$4.47 \pm 3.79 \times 10^{1}$
Bi	3.04 ± 4.20	$2.61 \pm 3.45 \times 10^{2}$	$1.54 \pm 0.99 \times 10^{3}$
Ca	$2.92 \pm 1.00 \times 10^{5}$	$6.33 \pm 3.17 \times 10^{3}$	$2.50 \pm 1.94 \times 10^{-2}$
Cd	$8.57 \pm 4.15 \times 10^{1}$	$3.87 \pm 4.68 \times 10^{2}$	6.60 ± 8.65
Ce	$2.79 \pm 2.83 \times 10^{1}$	$4.94 \pm 4.51 \times 10^{2}$	$1.96 \pm 0.38 \times 10^{1}$
Co	$3.58 \pm 4.00 \times 10^{1}$	$1.52 \pm 1.21 \times 10^{3}$	$6.27 \pm 3.62 \times 10^{1}$
Cr	$1.36 \pm 1.13 \times 10^{3}$	$9.35 \pm 1.17 \times 10^{2}$	1.00 ± 0.75
Cs	$2.88 \pm 0.08 \times 10^{4}$	$7.53 \pm 3.19 \times 10^{2}$	$2.60 \pm 1.04 \times 10^{-2}$
Cu	$4.63 \pm 3.23 \times 10^{1}$	$4.41 \pm 5.01 \times 10^{2}$	$1.76 \pm 2.31 \times 10^{1}$
Fe	1.81×10^{4} to 6.09×10^{4}	$1.32 \pm 0.54 \times 10^{4}$	2.17×10^{-1} - 7.28×10^{-1}
Ga	$6.00 \pm 8.24 \times 10^{5}$	$7.39 \pm 2.93 \times 10^{2}$	$1.54 \pm 2.06 \times 10^{-2}$
In	$7.92 \pm 9.51 \times 10^{1}$	$6.67 \pm 0.17 \times 10^{2}$	$2.98 \pm 3.56 \times 10^{1}$
K	$1.74 \pm 1.53 \times 10^{6}$	$1.64 \pm 0.93 \times 10^{6}$	1.92 ± 2.22
La	2.79 ± 3.29	$4.77 \pm 4.56 \times 10^{2}$	$2.44 \pm 1.24 \times 10^{2}$
Li	$4.52 \pm 2.84 \times 10^{3}$	$8.63 \pm 3.96 \times 10^{2}$	$2.04 \pm 0.40 \times 10^{-1}$
Mg	$7.81 \pm 5.56 \times 10^{3}$	$5.30 \pm 5.32 \times 10^{4}$	$1.23 \pm 1.56 \times 10^{1}$
Mn	$4.39 \pm 5.13 \times 10^{2}$	$1.00 \pm 1.26 \times 10^{4}$	$1.90 \pm 0.60 \times 10^{1}$
Mo	$1.17 \pm 0.21 \times 10^{7}$	$8.66 \pm 4.77 \times 10^{2}$	$7.56 \pm 2.88 \times 10^{-5}$
Ni	$2.92 \pm 1.63 \times 10^{2}$	$1.17 \pm 0.34 \times 10^{3}$	5.14 ± 4.01
Pb	$3.70 \pm 0.86 \times 10^{1}$	$4.06 \pm 2.67 \times 10^{2}$	$1.04 \pm 0.48 \times 10^{1}$
Rb	$8.75 \pm 1.57 \times 10^{4}$	$1.02 \pm 0.13 \times 10^{3}$	$1.20 \pm 0.36 \times 10^{-2}$
Sb	$1.02 \pm 1.37 \times 10^{3}$	$5.78 \pm 3.51 \times 10^{2}$	3.34 ± 4.14
Se	$2.21 \pm 0.58 \times 10^{6}$	$6.67 \pm 6.78 \times 10^{2}$	$3.54 \pm 4.00 \times 10^{-4}$
Sn	$1.24 \pm 0.61 \times 10^{8}$	$3.33 \pm 0.29 \times 10^{2}$	$2.99 \pm 1.24 \times 10^{-6}$
Sr	2.01 ± 0.01	$6.91 \pm 3.11 \times 10^{2}$	$3.40 \pm 1.38 \times 10^{2}$
Th	$1.09 \pm 1.53 \times 10^{1}$	$2.09 \pm 2.40 \times 10^{2}$	$4.01 \pm 5.43 \times 10^{2}$
Ti	$1.51 \pm 1.67 \times 10^{3}$	$6.22 \pm 2.19 \times 10^{2}$	$8.57 \pm 8.04 \times 10^{-1}$
Tl	$2.42 \pm 2.86 \times 10^{1}$	$6.16 \pm 2.66 \times 10^{2}$	$6.24 \pm 6.26 \times 10^{1}$

U	$0.79 \pm 1.09 \times 10^{3}$	$4.34 \pm 1.49 \times 10^{2}$	$0.8 \pm 1.08 \times 10^{1}$
V	2.47×10^{2}	5.19×10^{2}	1.05
Y	1.63 ± 2.05	$5.00 \pm 4.20 \times 10^{2}$	$6.82 \pm 5.99 \times 10^{2}$
Zn	$6.08 \pm 2.23 \times 10^{3}$	$1.86 \pm 0.58 \times 10^{2}$	$3.10 \pm 0.19 \times 10^{-2}$

Table 3. Known (extracted from the THERMODEM database) and experimental (measured in our study) partition coefficients ($logD^{X/Fe}$, with concentrations in solutions and magnetite expressed in molality and molar fractions respectively) between magnetite and the residual precipitation solution.

Element	Previously proposed $logD^{X/Fe}$	Measured $logD^{X/Fe}$ in abiotic magnetite
Co^{2+}	-0.8	-10.42 ± 0.19
Cu^{2+}	-10.32	-11.48 ± 0.22
Mn^{2+}	-14.91	-10.41 ± 0.01
Ni^{2+}	-9.78	-11.39 ± 0.24
Zn^{2+}	-11.73	-12.38 ± 0.59